Lin Han[1]
Biomedical Engineering,
Yale University,
Malone Center Room / space 103C,
55 Prospect Street,
New Haven, CT 06511
e-mail: han.lin@yale.edu

Jing Zhou[1]
Anesthesiology,
Yale School of Medicine,
Biomedical Engineering,
Yale University, Room 314,
10 Amistad Street,
New Haven, CT 06510
e-mail: jzjzhou@gmail.com

Yubing Sun
Mechanical Engineering,
University of Michigan,
2664 GGB (George G. Brown Laboratory),
2350 Hayward,
Ann Arbor, MI 48109-2125
e-mail: ybsun@umich.edu

Yu Zhang
Electrical Engineering,
Yale University,
15 Prospect Street,
New Haven, CT 06511
e-mail: yuzhang18@gmail.com

Jung Han
Electrical Engineering,
Yale University, Becton 517,
15 Prospect Street,
New Haven, CT 06511
e-mail: jung.han@yale.edu

Jianping Fu
Mem. ASME
Mechanical Engineering,
Biomedical Engineering,
University of Michigan,
2664 GGB (George G. Brown Laboratory),
2350 Hayward,
Ann Arbor, MI 48109-2125
e-mail: jphu@umich.edu

Rong Fan
Biomedical Engineering,
Yale University, Malone 213,
55 Prospect Street,
New Haven, CT 06511
e-mail: rong.fan@yale.edu

Single-Crystalline, Nanoporous Gallium Nitride Films With Fine Tuning of Pore Size for Stem Cell Engineering

Single-crystalline nanoporous gallium nitride (GaN) thin films were fabricated with the pore size readily tunable in 20–100 nm. Uniform adhesion and spreading of human mesenchymal stem cells (hMSCs) seeded on these thin films peak on the surface with pore size of 30 nm. Substantial cell elongation emerges as pore size increases to ~80 nm. The osteogenic differentiation of hMSCs occurs preferentially on the films with 30 nm sized nanopores, which is correlated with the optimum condition for cell spreading, which suggests that adhesion, spreading, and stem cell differentiation are interlinked and might be coregulated by nanotopography. [DOI: 10.1115/1.4030615]

1 Introduction

Nanostructured semiconductors with emerging optical or electronic properties have demonstrated wide-spread applications in microelectronics, optoelectronics [1–4], chemical [5,6] and biomolecular sensors [7–11], biomedical drug delivery [12], and biomolecular separation [13]. Recently, nanostructured surfaces are further opening new opportunities in rare cell analysis and stem cell engineering via nanoscale cell–surface interactions. Silicon or quartz nanowire substrates functionalized with antibodies against cell surface antigens were reported for high-efficiency rare cell capture [14] and hold great potential for clinical applications such as counting circulating tumor cells for differential diagnosis of cancer progression and metastasis [15]. Vertical silicon

[1]L. Han and J. Zhou contributed equally to this work.

Manuscript received February 2, 2015; final manuscript received March 17, 2015; published online June 24, 2015. Assoc. Editor: Donglei (Emma) Fan.

nanowires were exploited for physical delivery of genes or biomolecules into live cells [16]. The effect of nanoscale surface topography on the motility and vitality of cells is a topic of increasing interest. Cellular response to nanoscale topography has been studied using a range of surface nanotopologies [17–22] and nanobiomaterials [18,23]. Studies have shown that nanoscale cellular structures, such as focal adhesion and integrin, interact with the underlying topography of the substrate, which in turn affects cell behavior such as morphology, cell adhesion, cell spreading, motility, gene expression, and differentiation [19,22,24,25]. Nanotopography, with the feature size comparable to the functional cell adhesion structures, plays a unique role in regulating cell–surface interaction and subsequently mediating survival, proliferation, and differentiation of stem cells [26–31].

hMSCs are adult multipotent stem cells, which can differentiate into a variety of cell types, such as adipocytes, chondrocytes, and osteoblasts. By examining the cellular behavior of MSCs cultured in vitro on nanostructures, it provides new understanding of the effects that the nanostructures may have on the response and fate of stem cells. Such studies have been reported with ZrO_2 nanotube arrays [32], TiO_2 nanotube arrays [29,32], nanoporous and nanophase Al_2O_3 [33,34], and carbon nanotube (CNT) arrays [35]. It has been demonstrated that sub-100 nm topographies are more important in regulating adhesion and differentiation of hMSCs due in part to the nanoscale-engineered substrates creating microenvironments that mimic the physiological conditions and signal through the intracellular domains of the mechanosensing surface receptors [30,36,37]. Thus, nanostructured surface can directly modulate stem cell behavior and fate decision including proliferation and differentiation.

Here, we report the fabrication of single-crystalline nanoporous GaN substrate with tunable pore size. GaN is not only an optically active semiconductor but also relatively biocompatible and nontoxic [38]. We studied adhesion, spreading, and directed differentiation of hMSCs seeded on the surfaces of these new materials. We observed a size-dependent cell function and behavior. The differentiation of hMSCs is also shown to be coregulated by the substrate nanotopography.

2 Materials and Methods

2.1 Frication of GaN and GaN Nanoporous Films. The GaN films were grown on c-plane sapphire substrate using a two-step growth procedure by metal organic chemical vapor deposition [39]. Briefly, first, 20 nm GaN was deposited on the sapphire surface at 500 °C as the GaN epilayer. Then 2 μm unintentionally doped GaN was grown on top of this GaN epilayer, followed by 1–2 μm Si-doped GaN with $5 \times 10^{18}\,cm^{-3}$ doping concentration.

The nanoporous GaN films were fabricated by electrochemical etching [39,40]. In brief, the GaN films were soaked in the electrolyte (0.3 M Oxallic acid) at room temperature. An indium-contacted GaN film and a platinum wire were used as the anode and cathode, respectively. Constant voltage was applied to the film, and the resulting current change was used to monitor the etching progress. The pore size and the porosity of nanoporous GaN films were determined by the etching voltages and doping concentration of GaN. In our experiments, the doping concentration of GaN was fixed at $5 \times 10^{18}\,cm^{-3}$. The etching voltages were set at 10 V, 15 V, 20 V, and 25 V, to achieve different pore sizes, ranging from 20 nm to 95 nm. After etching, GaN films were rinsed in deionized water to remove residual reagents.

2.2 Scanning and Transmission Electron Microscopy. EM was used to characterize the microscale morphology and structure of nanoporous GaN films. GaN films with and without nanopores were diced into small species and bonded to metal holders with carbon tape. The surface and cross-sectional morphology of GaN films were characterized by the high-resolution scanning electron microscopy (SEM) (Hitachi SU-70). Thin nanoporous GaN films were lifted off from sapphire substrate for transmission electron microscopy (TEM) analysis. This process was a two-step electrochemical etching [39]. It began at the target voltage to generate nanopores with desired diameter. Once the required thickness of the lift-off layer is achieved, the etching voltage was increased to a higher value, e.g., > 25 V, to overetch the structure underneath the lift-off layer so that it can be easily released from the handle substrate. The lift-off GaN film was transferred onto a copper sample grid and characterized by TEM (Philips CM-12).

The SEM images were analyzed by CELLPROFILER 2.0 (Broad Institute, Cambridge, MA), image analysis software, to quantify the pore size and the porosity of nanoporous GaN films. The software distinguished the nanopores from the background based on the brightness and contrast of SEM images. It computes the total number of nanopores, the size of each nanopore, and the area occupied by each nanopore. The porosity of nanoporous GaN film was defined by the fill factor of the surface, i.e., the ratio of the total area occupied by nanopores to the whole surface area.

2.3 Cell Culture and Cell Adhesion Assay. hMSCs were purchased from Lonza and cultured in Poietics™ MSCGM (Lonza Group Ltd., Basel, Switzerland) to maintain their undifferentiated status. The cells were cultured at 37 °C with 5% CO_2. The hMSCs used in the experiments were at passage 3–7.

hMSCs were cultured both on plain GaN films and nanoporous GaN films with different pore sizes. Before cell seeding, the GaN films were sonicated in 70% ethanol for 1 hr to clean and sterilize the surface. Then the films were rinsed three times with culture media to remove residual alcohol. A polydimethylsiloxane (PDMS) slab, with holes 5 mm in diameter and 5 mm in depth, was adhered to the surface of GaN films to define the cell culture areas. Two thousand cells were seeded in each hole. The whole devices were incubated at 37 °C with 5% CO_2. At time point of 4 hrs and 24 hrs, the cells were fixed for further analysis.

2.4 Immunofluorescence Staining. For immunofluorescence staining, the hMSCs on the GaN films were fixed with 4% paraformaldehyde for 10 mins and then rinsed three times with 1 × phosphate buffered saline (PBS) (Invitrogen; Thermo Fisher Scientific Corp, Waltham, MA). The cells were blocked in blocking buffer (5% bovine serum albumin (Sigma-Aldrich St. Louis, MO) and 0.3% Triton X-100 (Sigma-Aldrich) in 1 × PBS) for 60 mins. After rinsed with 1 × PBS three times for 5 mins each, the actin filaments were stained with Alexa Fluor 647 conjugated phalloidin (Invitrogen) for 20 mins and the nuclei were stained with 4′,6-diamidino-2-phenylindole (DAPI) (cell signaling) for 5 mins.

2.5 Imaging Acquisition and Analysis. Bright field and fluorescence images of hMSCs on GaN films were collected under a fluorescent microscope with a charge-coupled device (CCD) camera (EVOS fl; Advanced Microscopy Group, Bothell, WA). All images in a given group were collected with the same hardware and software settings.

CELLPROFILER 2.0 was used to analyze the cell morphology. The nuclear staining was used to count the cell number. The actin filament staining was used to identify the cell shape and area. The elongation of hMSCs is defined by the ratio of the major axis to the minor axis of the cell.

2.6 MSC Osteogenic Differentiation. hMSCs (Lonza, Walkersville, MD) at passage two were seeded at a density of 2000 cells/cm^2 on GaN films. The osteogenic differentiation was induced by Osteogenesis differentiation medium (Lonza). hMSCs maintained in growth media were used as negative controls. Media were changed every two days and cells were stained seven days after seeding. Cells were fixed with citrate buffered acetone for 30 s and then rinsed gently with PBS. Alkaline phosphatase (ALP) activity was assessed using a leukocyte alkaline phosphatase kit (Sigma, St. Louis, MO) with fast blue RR (4-

Benzoylamino-2,5-dimethoxybenzenediazonium chloride hemi (zinc chloride)) salt, as described in Ref. [40]. Bright field images were obtained using a $10\times$ objective (0.3 NA, dry; Plan Fluor, Nikon Corp, Tokyo, Japan) on a Nikon E800 upright widefield microscope equipped with a color CCD camera.

2.7 Statistics. ANOVA analysis was used to analyze the morphology of hMSCs and the number of ALP^+ cells after osteogenesis differentiation on different GaN films. $P < 0.05$ was defined as significant difference with * mark in plot, and $p < 0.01$ was defined as very significant difference with ** mark in plot. For the morphology characterization, each condition has the number of cells analyzed > 100 except on plain GaN films (over 50 cells has been analyzed due to reduced cell adhesion on plain GaN films). At least four independent experiments were conducted to examine hMSC morphology on different GaN films. For the osteogenic differentiation, the number of cell evaluated is > 100 and at least three experiments were performed for each condition.

3 Results and Discussion

3.1 The Dependence of the Morphology and Structure of Nanoporous GaN Films on the Etching Voltage. The GaN substrates used in this study were n-type with a doping level of $5 \times 10^{18}\,cm^{-3}$. The electrochemical etching process was carried out under the applied voltage of 10, 15, 20, and 25 V, to generate etched nanopores on the GaN substrates. The topography of the resultant nanoporous GaN films was characterized by SEM (Fig. 1). When the etching voltage is too low, no formation of nanopores was observed. When the etching voltage is 25 V or higher, the GaN films become overetched, as indicated by the appearance of uneven surface (Fig. 1(*d*)). We found that the size and the density of the nanopores increase with the increase of the etching voltages as shown in Figs. 1(*a*)–1(*d*).

The nanopore size and the porosity of GaN nanoporous films were analyzed using CELL PROFILLER, an image analysis software, to quantify the SEM images, on which the nanopores appear

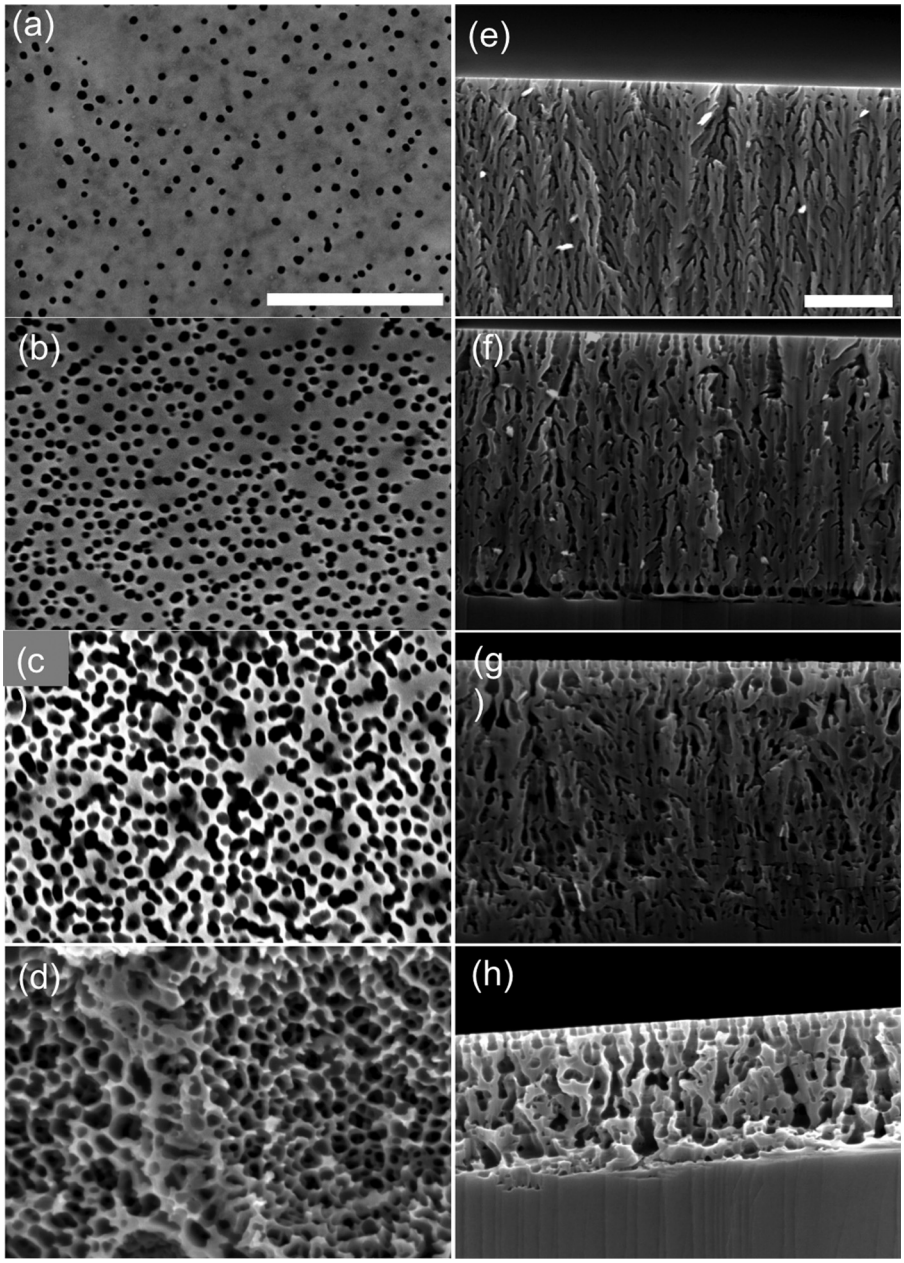

Fig. 1 SEM images of the top view (*a*)–(*d*) and the cross section (*e*)–(*h*) of nanoporous GaN films etched at 10 V, 15 V, 20 V, and 25 V. The scale bar is 500 nm.

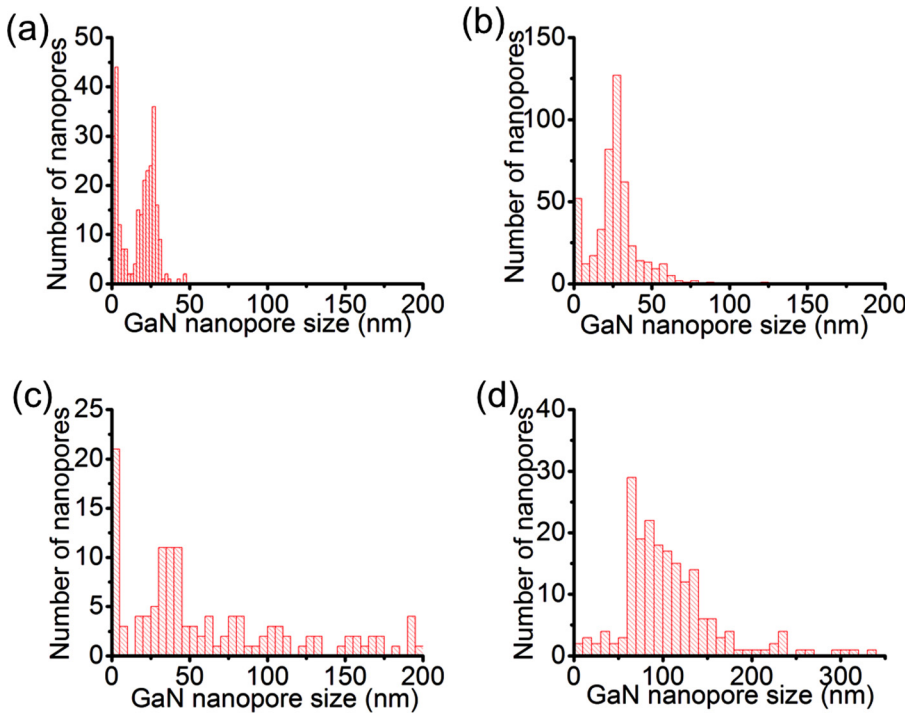

Fig. 2 Pore size distributions of GaN nanoporous films under different etching voltages: (*a*) 10 V, (*b*) 15 V, (*c*) 20 V, and (*d*) 25 V

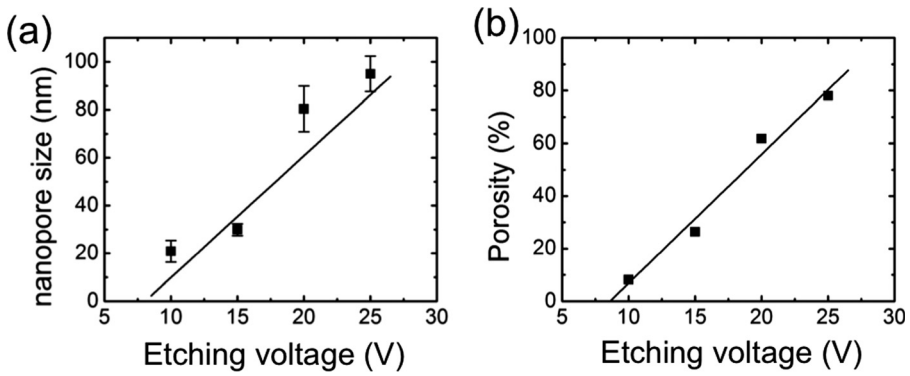

Fig. 3 The dependence of pore size (*a*) and porosity (*b*) on the etching voltages

darker than the flat surface regions. Based on the brightness and contrast of SEM images, CELLPROFILLER can identify the nanopores and calculate the total number of nanopores per surface area, the shape and the area of the nanopores. The size distributions of nanopores under different etching voltages are shown in Figs. 2(*a*)–2(*d*). The sizes of the nanopores in the films, etched at 10 V (Fig. 2(*a*)) and 15 V (Fig. 2(*b*)), are more uniform than those in the films etched at 20 V (Fig. 2(*c*)) and 25 V (Fig. 2(*d*)). The mean of nanopore sizes ramps up from 20, 30, 80, to 95 nm when the etching voltage increases from 10 to 15, 20, and 25 V (Fig. 3(*a*)). The porosity of the GaN film is defined as the fill factor—the ratio of the total area of nanopores to the area of the entire surface. The porosity ranges from 8% to 26%, 62%, and 78%, corresponding to the etching voltages of 10, 15, 20, and 25 V (Fig. 3(*b*)). Both nanopore size and the porosity of GaN films show a monotonic relation with the etching voltage.

The cross-sectional views (Figs. 1(*e*)–1(*h*)) show that the etching of the nanopores, instead of advancing straight through out the whole film, branches out and forms treelike structures. The width of the etching path also increases with the increase of the etching voltages. At low etching voltages, the anodic etching selectively occurs at the sharp ends of the nanopores. The etching direction advances approximately perpendicularly to the semiconductor/electrolyte interface or in parallel to the direction of electric field/current flow, resulting in narrow etching path. As the etching voltage increases, the electrochemical etching direction at the front end of the nanopores quickly ramifies and branches out in a successive manner, resulting in the generation of nanopores more parallel to the semiconductor/electrolyte interface and the wider etching path.

3.2 Single Crystal GaN Nanoporous Film. The crystallinity of nanoporous GaN layer was characterized by TEM. A typical TEM analysis of an as-etched GaN film is shown in Fig. 4. The surface of the GaN film is uniformly covered with nanopores with interconnected channels (Fig. 4(*a*)). The pore size is ~20 nm (doping concentration $= 5 \times 10^{18}\,\mathrm{cm}^{-3}$ and etching voltage $= 10$ V) (Fig. 4(*b*)). The selected-area diffraction (SAD) pattern

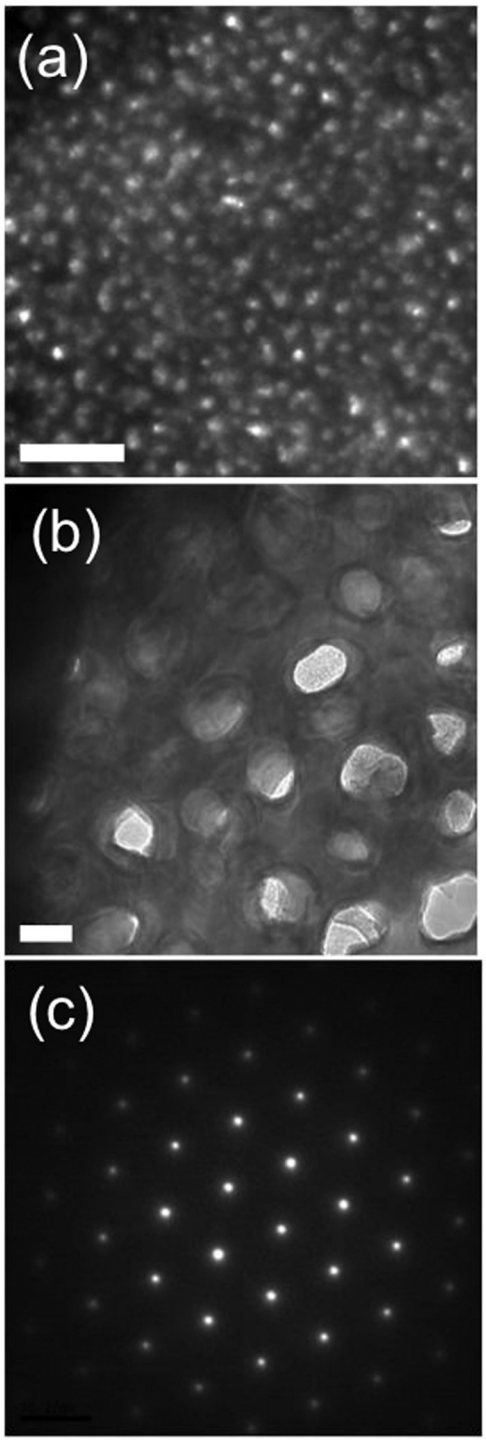

Fig. 4 TEM analysis of nanoporous GaN films. (*a*) The nanopores uniformly cover the surface of GaN film. (*b*) Higher magnification image shows the pore size is ~20 nm (doping concentration = 5×10^{18} cm^{-3} and etching voltage = 10 V). (*c*) Selected-area electron diffraction pattern (SAD) of the nanoporous GaN membrane shows the sixfold symmetry along the [0001] axis. The scale bar in (*a*) is 200 nm and (*b*) is 20 nm.

clearly shows a sixfold symmetry along the [0001] axis, indicating the single crystallinity of the film. Greater diffuse scattering appears around the beams, which is attributed to the large internal surface area of the GaN nanoporous film and the uncertainty principle [41].

3.3 MSC Adhesion and Spreading on GaN Films. The nanopore size and porosity are important in regulating the fate of cells seeded on the surface. In this work, the size and density of GaN nanopores can be readily tuned by varying the etching voltages and, if necessary, the doping density as well. At a given doping density, the pore size increases with the increase of etching voltage until it is too high and causes overetching. All these made our nanoporous GaN films an ideal platform comprising a series of nanoporous films with varying nanopore properties for systematic study of stem cell function modulated by cell–nanotopology interaction.

We investigated the cell adhesion and spreading on flat and nanoporous GaN films. The pore size of the nanoporous GaN films is 20, 30, 80, and 95 nm, corresponding to the porosity of 8%, 26%, 62%, and 78%. hMSCs were seeded on the GaN films, cultured for a given period of time (4 hrs or 24 hrs) to allow for cell adhesion and spreading to occur. Then, the cells on the GaN substrates will be fixed and strained for fluorescence microscopy study. The actin filaments of hMSCs were stained with Phalloidin, and the nuclei were stained with DAPI. We found that the morphology of hMSCs was strongly modulated by the nanotopography of the GaN substrate. After 4 hrs culture, hMSCs did not fully spread and remained round on the plain GaN films as well as the GaN films with 20 and 30 nm nanopores (Figs. 5(*a*)–5(*c*)). But on the GaN films with 80 and 95 nm nanopores, hMSCs already spread substantially and the lamellipodia extensions were readily observed (Figs. 5(*d*) and 5(*e*)). After 24 hrs culture, hMSCs spread on all nanoporous GaN films but not on the plain GaN films (Figs. 5(*f*)–5(*j*)). The hMSCs on nanoporous GaN films retain the typical hMSC morphology at the undifferentiated stage. For example, the cells on the GaN films with 30 and 80 nm nanopores appeared to be spindle-shaped, while the cells on the GaN films with 20 and 95 nm nanopores display a starlike/polygonlike shape.

The morphology of hMSCs cultured on the plain and nanoporous GaN films was quantified by CELLPROFILLER. The cell elongation is defined by the ratio of the major axis length of cell to the minor axis length of a cell. At 4 hrs culture, the cells have not completely adhered and spread on the substrate, showing smaller cell area compared to those after 24 hrs culture (Figs. 6(*a*) and 6(*c*)). On plain GaN films and nanoporous GaN films with 20 nm and 30 nm pores, the cells remain the round shape and the elongation index is close to one. The cells adhered and spread slightly after 4 hrs on the nanoporous GaN films with 80 nm and 95 nm pores, with the highest cell spreading area observed for the films with 80 nm nanopores (Figs. 6(*a*) and 6(*b*)). After 24 hrs culture, the cells spread on all nanoporous GaN films but still not on the plain GaN films (Fig. 6(*c*)). The largest spreading area of hMSCs was observed on GaN films with 30 nm nanopores (corresponding to 26% porosity). On other nanoporous GaN films, the cell spreading areas are similar. This is consistent with the literature results obtained with TiO_2 and ZrO_2 nanotube arrays, which suggests highest cell adhesion on nanotube array with diameter ~30 nm [29,32]. Significant cell elongation was only observed on the GaN films with pore sizes of 30 and 80 nm (corresponding to porosity of 26% and 62%), with the most significant elongation for the nanopore size of 80 nm (Fig. 6(*d*)). The cell elongation corresponding to the spindle shape of cells was retained on these nanoporous GaN films as shown in Figs. 5(*h*) and 5(*i*). This observation also agreed with studies with TiO_2 nanotube arrays, which showed the largest elongation on nanotube array with a diameter of ~70 nm [29,32].

3.4 MSC Osteogenic Differentiation on Nanoporous GaN Films. We also investigated the effect of pore size and porosity of nanoporous GaN films on hMSC osteogenic differentiation, which is one of the major potential applications of hMSCs in tissue engineering. We cultured hMSCs on nanoporous GaN films with osteogenic differentiation media for seven days. The nanopore diameters of these substrates are 20, 30, 80, and 95 nm, corresponding to porosities of 8%, 26%, 62%, and 78%. After seven days, we assessed osteogenesis by detecting ALP expression with Fast Blue RR salt. Figure 7(*a*) shows the representative images of

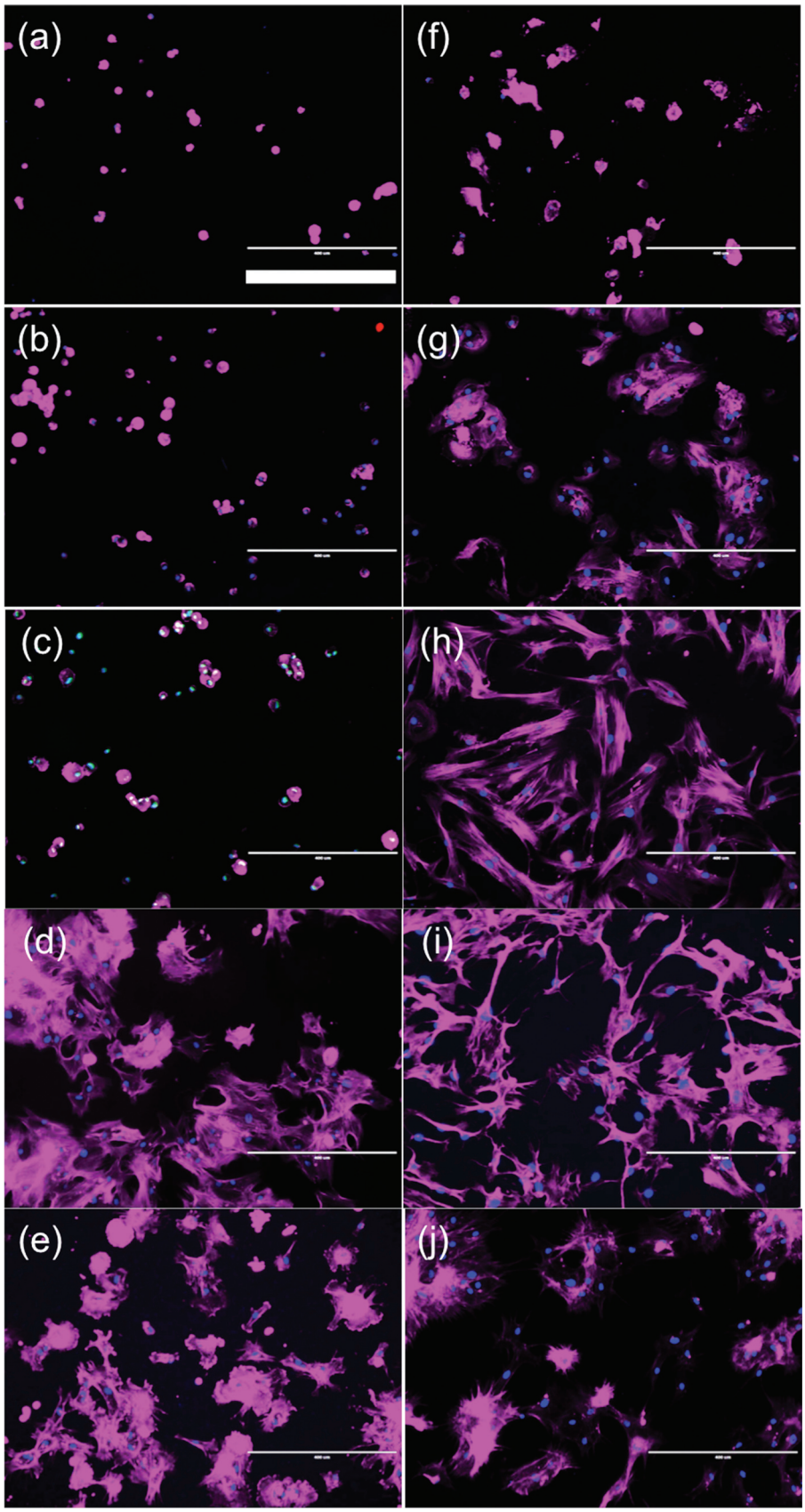

Fig. 5 hMSCs adhesion and spreading on GaN films with and without nanopores. Immunofluorescent images of hMSCs on (*a*) plain GaN film, and GaN films with (*b*) 20 nm, (*c*) 30 nm, (*d*) 80 nm, and (*e*) 95 nm nanopores, after 4 hrs culture; on (*f*) plain GaN film, and GaN films with (*g*) 20 nm, (*h*) 30 nm, (*i*) 80 nm, and (*j*) 95 nm nanopores, after 24 hrs culture. The scale bar is 400 μm.

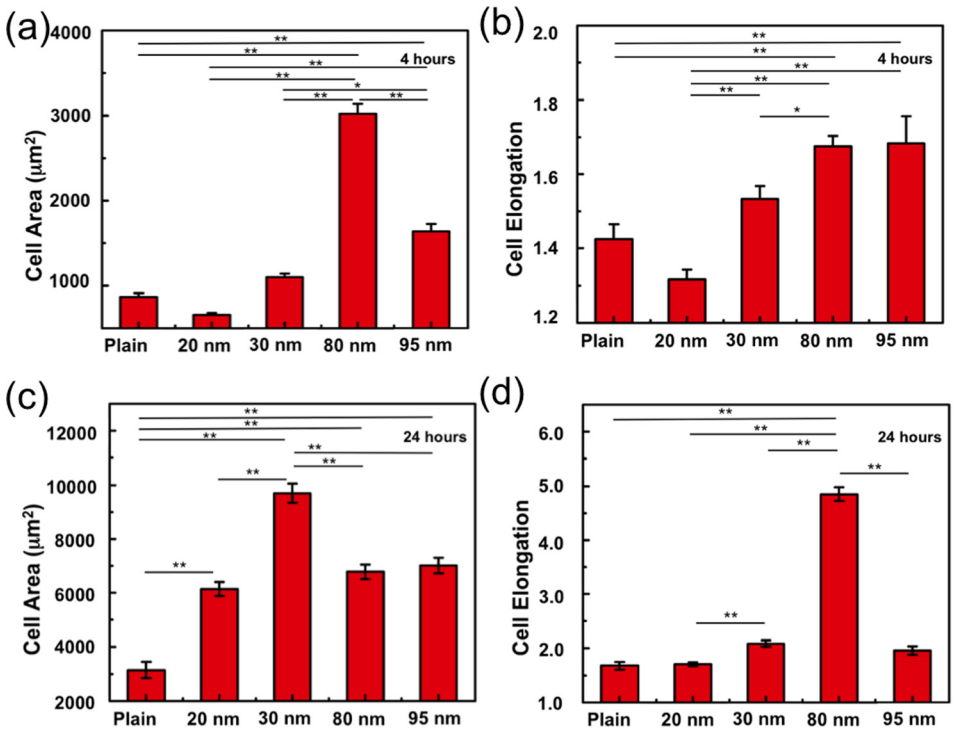

Fig. 6 Quantify the morphology of hMSCs cultured on the plain and nanoporous GaN films with different pore sizes: the spreading area (*a*) and the elongation (*b*) of cells after 4 hrs culture; the spreading area (*c*) and the elongation (*d*) of cells after 24 hrs culture. * = significant at 5% level; ** = significant at 1% level.

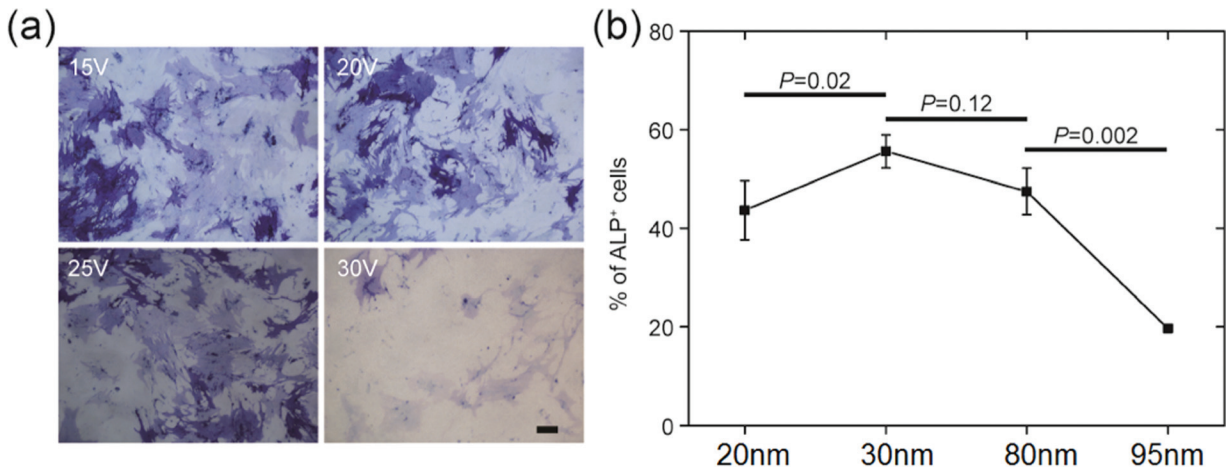

Fig. 7 (*a*) Brightfield images of hMSCs cultured in osteogenesis media on nanoporous GaN films for seven days and ALP was stained with fast blue RR salt. (*b*) Quantification of percentage of ALP$^+$ cells cultured on naoporous GaN substrates. The scale bar is 100 μm.

hMSCs stained for ALP. Staining intensity is indicative of ALP activity.

For substrates with nanopores larger than 30 nm, the percentage of cells expressing ALP decreased with increasing pore size and porosity. However, for small pore sizes (20–30 nm) the proportion of ALP+ cells increased with increasing pore size. Under the conditions we tested, GaN films with nanopores of 30 nm most effectively supported osteogenic differentiation. These results suggest that osteogenic differentiation on GaN can be modulated by the interaction between cells and nanostucture substrates. The observed optimum condition corresponds to the substrate with 30 nm nanopores and moderate porosity, i.e., 26%. The dependence of ALP expression on low and high porosity substrates correlate with the aforementioned results in cell elongation and spreading area as shown in Fig. 6. This indicates a possible mechanistic connection between cell elongation, cell spreading area, and osteogenic differentiation of mesenchymal stem cells. The most drastic change in ALP expression occurred between 80 nm and 95 nm, the latter of which exhibited the minimum percentage of ALP+ cells. For substrate with 95 nm nanopores, the GaN layer has been overetched, creating an uneven surface and loose branching morphology, as shown in Fig. 1. This topography appears to discourage osteogenic differentiation.

4 Conclusion

In this work, we report a simple and efficient approach—electrochemical etching—to fabricate the biocompatible

nanoporous GaN films for the study of cell adhesion, spreading, and surface-modulated differentiation. We can tune the pore size and porosity by varying the etching voltage. We fabricated nanoporous GaN films with the pore size ranging from 20 to 100 nm and with the porosity between 10 and 80%. We investigated cell adhesion, spreading, and differentiation of hMSCs on these nanoporous films. Cell adhesion and spreading exhibit a strong dependence on the size of the nanopores and the porosity of the nanoporous GaN films. hMSCs on GaN films with 30 nm nanopores (26% porosity) showed the largest spreading area, while those on GaN films with 80 nm nanopores (60% porosity) showed the largest elongation. Cell shape is a regulator of stem cell fate both in vivo and in vitro. We therefore investigated the hMSC osteogenic differentiation on these nanoporous GaN films. The osteogenic differentiation on GaN occurs preferentially on films with 30 nm sized nanopores (26%), which is correlated with the condition that permits the most effective cell spreading, suggesting the hMSC osteogenesis could be modulated by the nanotopography of the substrates, e.g., the nanoscale structure of nanoporous GaN films, which can be in turn employed to engineer stem cell fate. Further study of the mechanotransduction of hMSCs on nanoporous GaN films could provide new insights into the mechanisms with regard to how mesenchymal stem cell differentiation is regulated by the nanotopologic cues in the physiological microenvironment.

Acknowledgment

We also acknowledge the Yale Institute for Nanoscience and Quantum Engineering (YINQE) and the Yale Nanofabrication Center to allow us to use their facilities. This study was supported by National Science Foundation (NSF) under Award No. CMMI-1129964 (to J. H.), the Yale University Provost's Office Research Support (to J. Z.) and the U.S. National Cancer Institute Howard Temin Pathway to Independence Award (NIH R00 CA136759 to R. F.).

References

[1] Collins, R. T., Fauchet, P. M., and Tischler, M. A., 1997, "Porous Silicon: From Luminescence to LEDs," Phys. Today, **50**(1), pp. 24–31.
[2] Lazarouk, S., Jaguiro, P., Katsouba, S., Masini, G., La Monica, S., Maiello, G., and Ferrari, A., 1996, "Stable Electroluminescence From Reverse Biased n-Type Porous Silicon-Aluminum Schottky Junction Device," Appl. Phys. Lett., **68**(15), pp. 2108–2110.
[3] Richter, A., Steiner, P., Kozlowski, F., and Lang, W., 1991, "Current-Induced Light-Emission From a Porous Silicon Device," IEEE Electron Device Lett., **12**(12), pp. 691–692.
[4] Steiner, P., Kozlowski, F., and Lang, W., 1993, "Light-Emitting Porous Silicon Diode With an Increased Electroluminescence Quantum Efficiency," Appl. Phys. Lett., **62**(21), pp. 2700–2702.
[5] Foucaran, A., Pascal-Delannoy, F., Giani, A., Sackda, A., Combette, P., and Boyer, A., 1997, "Porous Silicon Layers Used for Gas Sensor Applications," Thin Solid Films, **297**(1–2), pp. 317–320.
[6] Sailor, M. J., and Link, J. R., 2005, "'Smart Dust': Nanostructured Devices in a Grain of Sand," Chem. Commun., **21**(11), pp. 1375–1383.
[7] Chan, S., Fauchet, P. M., Li, Y., Rothberg, L. J., and Miller, B. L., 2000, "Porous Silicon Microcavities for Biosensing Applications," Phys. Status Solidi A, **182**(1), pp. 541–546.
[8] Coffer, J. L., Whitehead, M. A., Nagesha, D. K., Mukherjee, P., Akkaraju, G., Totolici, M., Saffie, R. S., and Canham, L. T., 2005, "Porous Silicon-Based Scaffolds for Tissue Engineering and Other Biomedical Applications," Phys. Status Solidi A, **202**(8), pp. 1451–1455.
[9] Lin, V. S. Y., Motesharei, K., Dancil, K. P., Sailor, M. J., and Ghadiri, M. R., 1997, "A Porous Silicon-Based Optical Interferometric Biosensor," Science, **278**(5339), pp. 840–843.
[10] Thust, M., Schöning, M. J., Frohnhoff, S., Arens-Fischer, R., Kordos, P., and Lüth, H., 1996, "Porous Silicon as a Substrate Material for Potentiometric Biosensors," Meas. Sci. Technol., **7**(1), pp. 26–29.
[11] Dancil, K. P. S., Greiner, D. P., and Sailor, M. J., 1999, "A Porous Silicon Optical Biosensor: Detection of Reversible Binding of IgG to a Protein A-Modified Surface," J. Am. Chem. Soc., **121**(34), pp. 7925–7930.
[12] Haidary, S. M., Corcoles, E. P., and Ali, N. K., 2012, "Nanoporous Silicon as Drug Delivery Systems for Cancer Therapies," J. Nanomater., **2012**, p. 830503.
[13] Ileri, N., Létant, S. E., Britten, J., Nguyen, H., Larson, C., Zaidi, S., Palazoglu, A., Faller, R., Tringe, J. W., and Stroeve, P., 2009, "Efficient Nanoporous Silicon Membranes for Integrated Microfluidic Separation and Sensing Systems," MRS Proc., **1191**, pp. 87–92.
[14] Kim, S. T., Kim, D.-J., Kim, T.-J., Seo, D.-W., Kim, T.-H., Lee, S.-Y., Kim, K., Lee, K.-M., and Lee, S.-K., 2010, "Novel Streptavidin-Functionalized Silicon Nanowire Arrays for CD4(+) T Lymphocyte Separation," Nano Lett., **10**(8), pp. 2877–2883.
[15] Lee, S. K., Kim, G.-S., Wu, Y., Kim, D.-J., Lu, Y., Kwak, M., Han, L., Hyung, J.-H., Seol, J.-K., Sander, C., Gonzalez, A., Li, J., and Fan, R., 2012, "Nanowire Substrate-Based Laser Scanning Cytometry for Quantitation of Circulating Tumor Cells," Nano Lett., **12**(6), pp. 2697–2704.
[16] Shalek, A. K., Robinson, J. T., Karp, E. S., Lee, J. S., Ahn, D.-R., Yoon, M.-H., Sutton, A., Jorgolli, M., Gertner, R. S., Gujral, T. S., MacBeath, G., Yang, E. G., and Park, H., 2010, "Vertical Silicon Nanowires as a Universal Platform for Delivering Biomolecules Into Living Cells," Proc. Natl. Acad. Sci. U. S. A., **107**(5), pp. 1870–1875.
[17] Andersson, A. S., Bäckhed, F., von Euler, A., Richter-Dahlfors, A., Sutherland, D., and Kasemo, B., 2003, "Nanoscale Features Influence Epithelial Cell Morphology and Cytokine Production," Biomaterials, **24**(20), pp. 3427–3436.
[18] Dalby, M. J., Riehle, M. O., Johnstone, H. J., Affrossman, S., and Curtis, A. S., 2002, "Polymer-Demixed Nanotopography: Control of Fibroblast Spreading and Proliferation," Tissue Eng., **8**(6), pp. 1099–1108.
[19] Dalby, M. J., Yarwood, S. J., Riehle, M. O., Johnstone, H. J., Affrossman, S., and Curtis, A. S., 2002, "Increasing Fibroblast Response to Materials Using Nanotopography: Morphological and Genetic Measurements of Cell Response to 13-nm-High Polymer Demixed Islands," Exp. Cell Res., **276**(1), pp. 1–9.
[20] Rice, J. M., Hunt, J. A., Gallagher, J. A., Hanarp, P., Sutherland, D. S., and Gold, J., 2003, "Quantitative Assessment of the Response of Primary Derived Human Osteoblasts and Macrophages to a Range of Nanotopography Surfaces in a Single Culture Model In Vitro," Biomaterials, **24**(26), pp. 4799–4818.
[21] Riehle, M. O., Dalby, M. J., Johnstone, H., MacIntosh, A., and Affrossman, S., 2003, "Cell Behaviour of Rat Calvaria Bone Cells on Surfaces With Random Nanometric Features," Mater. Sci. Eng., C, **23**(3), pp. 337–340.
[22] Dalby, M. J., Gadegaard, N., Riehle, M. O., Wilkinson, C. D., and Curtis, A. S., 2004, "Investigating Filopodia Sensing Using Arrays of Defined Nano-Pits Down to 35 nm Diameter in Size," Int. J. Biochem. Cell Biol., **36**(10), pp. 2005–2015.
[23] Dalby, M. J., Riehle, M. O., Johnstone, H. J., Affrossman, S., and Curtis, A. S., 2003, "Nonadhesive Nanotopography: Fibroblast Response to Poly(n-Butyl Methacrylate)-Poly(Styrene) Demixed Surface Features," J. Biomed. Mater. Res., Part A, **67A**(3), pp. 1025–1032.
[24] Goldberg, D. J., and Burmeister, D. W., 1986, "Stages in Axon Formation-Observations of Growth of Aplysia Axons in Culture Using Video-Enhanced Contrast-Differential Interference Contrast Microscopy," J. Cell Biol., **103**(5), pp. 1921–1931.
[25] Polinsky, M., Balazovich, K., and Tosney, K. W., 2000, "Identification of an Invariant Response: Stable Contact With Schwann Cells Induces Veil Extension in Sensory Growth Cones," J. Neurosci., **20**(3), pp. 1044–1055.
[26] Yim, E. K. F., Reano, R. M., Pang, S. W., Yee, A. F., Chen, C. S., and Leong, K. W., 2005, "Nanopattern-Induced Changes in Morphology and Motility of Smooth Muscle Cells," Biomaterials, **26**(26), pp. 5405–5413.
[27] Dalby, M. J., Gadegaard, N., Tare, R., Andar, A., Riehle, M. O., Herzyk, P., Wilkinson, C. D. W., and Oreffo, R. O. C., 2007, "The Control of Human Mesenchymal Cell Differentiation Using Nanoscale Symmetry and Disorder," Nat. Mater., **6**(12), pp. 997–1003.
[28] Yim, E. K. F., Pang, S. W., and Leong, K. W., 2007, "Synthetic Nanostructures Inducing Differentiation of Human Mesenchymal Stem Cells Into Neuronal Lineage," Exp. Cell Res., **313**(9), pp. 1820–1829.
[29] Oh, S., Brammer, K. S., Li, Y. S., Teng, D., Engler, A. J., Chien, S., and Jin, S., 2009, "Stem Cell Fate Dictated Solely by Altered Nanotube Dimension," Proc. Natl. Acad. Sci. U. S. A., **106**(7), pp. 2130–2135.
[30] McMurray, R. J., Gadegaard, N., Tsimbouri, P. M., Burgess, K. V., McNamara, L. E., Tare, R., Murawski, K., Kingham, E., Oreffo, R. O. C., and Dalby, M. J., 2011, "Nanoscale Surfaces for the Long-Term Maintenance of Mesenchymal Stem Cell Phenotype and Multipotency," Nat. Mater., **10**(8), pp. 637–644.
[31] Yim, E. K. F., Darling, E. M., Kulangara, K., Guilak, F., and Leong, K. W., 2010, "Nanotopography-Induced Changes in Focal Adhesions, Cytoskeletal Organization, and Mechanical Properties of Human Mesenchymal Stem Cells," Biomaterials, **31**(6), pp. 1299–1306.
[32] Bauer, S., Park, J., Faltenbacher, J., Berger, S., von der Mark, K., and Schmuki, P., 2009, "Size Selective Behavior of Mesenchymal Stem Cells on ZrO_2 and TiO_2 Nanotube Arrays," Integr. Biol., **1**(8–9), pp. 525–532.
[33] Webster, T. J., Ergun, C., Doremus, R. H., Siegel, R. W., and Bizios, R., 2000, "Enhanced Functions of Osteoblasts on Nanophase Ceramics," Biomaterials, **21**(17), pp. 1803–1810.
[34] Popat, K. C., Chatvanichkul, K. I., Barnes, G. L., Latempa, T. J., Jr., Grimes, C. A., and Desai, T. A., 2007, "Osteogenic Differentiation of Marrow Stromal Cells Cultured on Nanoporous Alumina Surfaces," J. Biomed. Mater. Res., Part A, **80A**(4), pp. 955–964.
[35] Kim, J. A., Jang, E. Y., Kang, T. J., Yoon, S., Ovalle-Robles, R., Rhee, W. J., Kim, T., Baughman, R. H., Kim, Y. H., and Park, T. H., 2012, "Regulation of Morphogenesis and Neural Differentiation of Human Mesenchymal Stem Cells Using Carbon Nanotube Sheets," Integr. Biol., **4**(6), pp. 587–594.
[36] Kim, S. J., Lee, J. K., Kim, J. W., Jung, J. W., Seo, K., Park, S. B., Roh, K. H., Lee, S. R., Hong, Y. H., Kim, S. J., Lee, Y. S., Kim, S. J., and Kang, K. S., 2008, "Surface Modification of Polydimethylsiloxane (PDMS) Induced

Proliferation and Neural-Like Cells Differentiation of Umbilical Cord Blood-Derived Mesenchymal Stem Cells," J. Mater. Sci.: Mater. Med., **19**(8), pp. 2953–2962.
[37] Park, J., Bauer, S., von der Mark, K., and Schmuki, P., 2007, "Nanosize and Vitality: TiO_2 Nanotube Diameter Directs Cell Fate," Nano Lett., **7**(6), pp. 1686–1691.
[38] Jewett, S. A., Makowski, M. S., Andrews, B., Manfra, M. J., and Ivanisevic, A., 2012, "Gallium Nitride is Biocompatible and Non-Toxic Before and After Functionalization With Peptides," Acta Biomater., **8**(2), pp. 728–733.
[39] Zhang, Y., Ryu, S.-W., Yerino, C., Leung, B., Sun, Q., Song, Q., Cao, H., and Han, J., 2010, "A Conductivity-Based Selective Etching for Next Generation GaN Devices," Phys. Status Solidi B, **247**(7), pp. 1713–1716.
[40] Zhang, Y., Sun, Q., Leung, B., Simon, J., Lee, M. L., and Han, J., 2011, "The Fabrication of Large-Area, Free-Standing GaN by a Novel Nanoetching Process," Nanotechnology, **22**(4), p. 045603.
[41] Cullis, A. G., and Canham, L. T., 1991, "Visible-Light Emission Due to Quantum Size Effects in Highly Porous Crystalline Silicon," Nature, **353**(6342), pp. 335–338.